Influence of Surface Wettability on Methane Hydrate Formation in Hydrophilic and Hydrophobic Mesoporous Silicas

Mirian E. Casco,[a*] *Sven Grätz,*[b] *Dirk Wallacher,*[c] *Nico Grimm,*[c] *Daniel M. Többens,*[c] *Malina Bilo*[d], *Natascha Speil*[d], *Michael Fröba*[d] *and Lars Borchardt,*[b]

[a]Department of Engineering, Catholic University of Uruguay, Av. 8 de Octubre, 2738, 11600 Montevideo, Uruguay

[b]Inorganic Chemistry, Ruhr-University Bochum, 44801 Bochum, Germany

[c]Helmholtz-Zentrum Berlin für Materialien und Energie (HZB), Hahn-Meitner-Platz 1, 14109 Berlin, Germany

[d] Institute of Inorganic and Applied Chemistry, University of Hamburg, Martin-Luther-King-Platz 6, 20146 Hamburg, Germany

E-mails corresponding authors: mirian.casco@ucu.edu.uy

ABSTRACT. The methane hydrate (MH) formation process in confinement was investigated using high-pressure methane sorption experiments on two wet materials with similar pore size distributions, B – PMO (hydrophobic) and MCM – 41 (hydrophilic). Their methane sorption isotherms possess two discrete methane gas consumption steps at ~10 bar and ~30 bar at 243 K. A systematic analysis reveals that external water and the so-called 'core water' inside the pore is rapidly consumed in the first step to form bulk-like hydrate, whereas adsorbed water is slowly consumed in the second step to form less stable confined hydrates at higher pressures. Synchrotron powder X-Ray results confirm methane hydrate structure I and reveal that bulk ice is swiftly and fully converted to hydrate in MCM – 41, whereas inactive bulk ice co-exists with MH

in B – PMO at 6 MPa demonstrating the huge impact of the surface wettability on the water's behavior during MH formation.

Keywords. Mesoporous silica; methane hydrate; confinement; wettability

1. INTRODUCTION

Methane, the main component of natural gas, is the cleanest energy source among hydrocarbons[1] and it is stored in massive amounts as hydrate in regions of permafrost and beneath the sea in outer continental margins. The estimation suggests 1600-1800 Gt of carbon surpassing the rest of carbon fossil fuels in Earth.[2,3] If the world could take advantage of this gas resource, the global energy landscape would change. In this context, much effort has been put towards the realization of safe and practical methods for methane mining from these regions as well as for its storage and transportation.[4,5] Since the methane molecule is a highly active greenhouse gas, the uncontrolled release of methane from the permafrost would be catastrophic for the climate. This work provides additional basic information about the formation and stability of methane hydrates in nanopores which also occur in nature, contributing, at the end, to avoid the uncontrolled release.

A gas hydrate is a non-stoichiometric inclusive compound in which the gas molecules (guest) are trapped inside well-defined cages formed by hydrogen-bonded water molecules (host). Gas hydrates generally have three structures depending on the nature and size of the guest: structure I, II and H. Structure I is most common one, found in nature for methane and natural gas, with the ideal stoichiometry of $CH_4 \cdot 5.75H_2O$.[6] Owing to the slow kinetics of formation, several scientists have reported on different methodologies to form methane hydrate (MH) in the laboratory within a reasonable time scale,[7–10] including the construction of innovative reactor configurations (stirred tank, bubble column, spray reactor), the incorporation of thermodynamic (e.g. THF)[11,12] and/or kinetics promoters (e.g. anionic, cationic and nonionic surfactants, amino acids) in the

system.[13,14] The use of different materials like silica gel[15], silica sand,[16] activated carbon[17,18], dry water,[19] zeolite,[20] hollow silica,[21] MOFs,[22,23] clays[24] have been also investigated to improve the gas-liquid interface in a unstirred fixed bed to enhance the kinetics of the process. [25]

The evaluation of confined MH formation has been further motivated by the necessity to understand the natural process, where gas hydrates grow in bearing sediments. Though proof of concept has been established, the mechanisms of nucleation and growth in confinement is complex and, until now, it is not clearly understood. Several factors affect the nucleation in confinement, including the level of gas saturation, the surface wettability, and the water activity. These parameters are mainly determined by the surface chemistry and the pore size and geometry of the selected porous materials. For instance, experiments using wet hydrophobic porous carbons have shown to diminish the induction time (periods when nuclei forms) from days to minutes.[25] Moreover, the extremely efficient pore interconnectivity between micro- meso-, and macropores allows for a complete water-to-hydrate conversion and even non-freezable water in narrow micropores is prone to form MH in this environment.[26] In contrary, experiments on microporous zeolites and microporous MOFs have demonstrated that even though the pore surface offers nucleation sites for MH, the crystals growing process occurs on the external surface, where there are no space limitations.[20,22] Recently, we have shown that the physical properties of confined water, such as mobility and phase state, has a tremendous impact on the water-to-hydrate conversion. For instance, MH crystals form from confined liquid water in hydrophobic ordered mesoporous carbons but are then decomposed into ice on the pore mouths or on the external surface, while in a hydrophilic ordered mesoporous carbon, the liquid water in pores is not prone to form MH. Moreover, the kinetics is affected by the ice phase, with preliminary results indicating that stacking disorder ice (formed in hydrophilic pores) is preferential to speed up the MH formation.[18]

Despite we have shown the huge impact of hydrophilicity and hydrophobicity on MH formation in carbons, silicates is the basic component of rock where most methane hydrate is found, and silica can serve as a first model compound without surface charges and charge-compensating metal ions to mimic nature at laboratory-scale. Therefore, it is fundamental to study the impact of polarity in silica on confined water and methane hydrate formation process. The physical properties of confined water in mesoporous silica, such as the depression of the melting/freezing point, have been widely addresses in literature.[27–29] Mietner et al. have further studied the effects of the surface polarity on the properties of spatially confined water in periodic mesoporous organosilicas (PMOs).[30] PMOs combine highly ordered pore structure with well-defined surface chemistry within cylindrical pores offering an ideal scenario to further investigate their effects on MH formation process.

PMOs are synthesized using bissilylated organosilica precursors of the form $(R'O)_3Si\text{-}R\text{-}Si(OR')_3$ where R is an organic bridging group which can be altered according to the desired surface properties.[31] While traditional ordered organosilicas includes post-synthetic grafting that decreases pore size and an uncontrolled distribution of the organic functionalities, PMOs are synthetized by one-pot reactions where every single-source precursor contains an organic functional group resulting in a homogeneous distribution of the organic moieties throughout the silica matrix and a highly ordered pore structure.[32] Mietner et al. have investigated by multidimensional solid state NMR the molecular mobility of water confined in PMOs and MCM - 41. Experiments showed the spatial arrangement of water inside the pores, demonstrating that water interacts either with only the silica unit (uniform pore filling mode on MCM - 41 surface) or with both silica and organic units (modulated pore filling mode on PMO surface) depending on the alternating surface polarity.[30]

Based on this knowledge, in this work, we select MCM – 41 and benzene bridged PMO materials (B – PMO) possessing practically identical pore structures and well-defined surface chemistry as ideal model system to explore the impact of alternating adsorbed confined water on the mechanisms of methane hydrate nucleation and growth in confinement. The evolution of the methane consumption with pressure at three temperatures for dry and wet samples is investigated by high-pressure sorption experiments. Synchrotron powder X-ray experiments are performed to provide structural information on the methane hydrate crystal. Finally, a model of water and hydrate distribution in porous media will be proposed.

2. MATERIALS AND METHODS

2.1 Synthesis and characterization of MCM - 41 and B - PMO

Parent MCM – 41 silica was prepared according to a slightly modified form of the previously published procedure of Lin et al.[33] For this purpose, 2.19 g of hexadecyl-trimethylammonium bromide were dissolved in a mixture of 30 mL of demineralized water and 2.8 mL of aqueous ammonia (25 wt.%) under stirring at 35 °C. After cooling down to room temperature, 2.5 mL of tetraethyl orthosilicate were rapidly added to the alkaline surfactant solution and the reaction mixture was stirred for two hours, before it was hydrothermally treated in a Teflon-lined autoclave for 48 hours, that was placed within an oven at 100 °C under static conditions. The resulting product was obtained by filtration, washed with 500 mL of demineralized water and 50 mL of ethanol and dried up to mass constancy at 60 °C. The surfactant CTAB was removed by subsequent calcination under air for 6 h at 550 °C with a heating rate of 1.5 $K \cdot min^{-1}$. 1,4-Bis(triethoxysilyl)benzene (BTEB) was synthesized according to the literature.[34] The B – PMO powder was prepared according to the following procedure. Sodium hydroxide (0.86 g) and octadecyltrimethylammonium chloride (1.72 g) were dissolved in distilled water (56 g) at 40 °C.

The mixture was cooled down to room temperature and BTEB (2 mL) was added. This mixture was stirred over night at room temperature in a glass bottle with screw cap and subsequently treated at 100 °C under static conditions for 24 h. The precipitate was isolated by filtration and washed with water and ethanol. The surfactant was removed by Soxhlet extraction. For the extraction a mixture of ethanol and hydrochloric acid 32 wt% (97/3, *v*/*v*) was used as solvent. Afterwards, the organosilica material was dried.[30] The porosity and the pore structure of the dried materials were characterized by powder X-ray diffraction and nitrogen adsorption. Powder X-ray diffractograms (P-XRD) were recorded at room temperature in θ/θ geometry with filtered $Cu_{K\alpha 1}$ radiation of 45 kV, 40 mA and a wavelength of 0.154 nm using an *X'Pert Pro MPD* from *PANalytical*. The measurement time was 500 s per step at a step width of 0.013° 2θ in the range of 0.5–10° 2θ. The evaluation of the X-ray powder diffractograms was carried out using the *X'Pert HighScore Plus* software from *PANalytical*. Prior to the gas physisorption measurements all samples were outgassed on a *Quantachrome Degasser Masterprep*® under vacuum for 20 h at 80 °C for organosilica and 120 °C for pristine silica. Then nitrogen physisorption isotherms were measured at 77 K in a relative pressure range from 0.02 to 0.99 with an *Autosorb® 6B* or a *Quadrasorb®-SI-MP* from *Quantachrome Instruments*. Pore size distributions and pore diameters D_{pore} were determined by evaluation with the *QuadraWin™* 6.0 software from *Quantachrome Instruments* using the non-local density functional theory (NLDFT) model. For these mesoporous silica materials, the kernel *N_2 at 77 K on silica (cylindrical pore, NLDFT, adsorption branch)* was used.[35] The total pore volume V_{total} was calculated at a relative pressure of 0.97, whereas the specific surface area S_{BET} was determined using the method by Brunauer, Emmett and Teller (BET)[36] in the relative pressure range from 0.02 to 0.3. Water vapor sorption measurements were carried out at 298 K with *Quantachrome Vstar™* vapor sorption analyzer using *VstarWin* 1.1.6 for analysis.

Prior to the water impregnation process both samples were degassed at 200 °C for 12 h. Afterwards the silica were loaded with water up to reach 80% or 150% of the total pore volume. The total pore volume was taken from the nitrogen isotherm data. The cooling/heating scans of the confined water were analysed in *DSC Mettler Toledo* instrument in a temperature range of 190 K to 290 K using a rate of 1 K min^{-1}. High pressure methane adsorption measurements were performed at 243 K, 258 K and 275 K up to 6 MPa using a volumetric BELSORP-HP apparatus.

2.2 Synchrotron powder X-ray diffraction

Combined powder X-ray diffraction experiments during the adsorption of methane were conducted at KMC-2 beamline of BESSY II light source of HZB (Helmholtz-Zentrum Berlin für Materialen und Energie).[41] A capillary-based sample cell, centred in the synchrotron beam, was connected to a gas dosing system (Teledyne ISCO9 pump controller). An alternate 180° rotation of the capillary in the beam was implemented by using a script-controlled step motor. The temperature of the sample was directly measured by K-type thermocouple, mounted close to the measurement point and connected to a Eurotherm indicator unit 32h8i. The tempering of the sample was provided by a nitrogen flow cooler N-Helix (Oxford Cryosystems). The gas jet temperature is software controller (Labview). The output of the software loop (calculated by a PID equation with sample temperature and set points as inputs) is the set points of the gas jet temperature (cascade control). A 0.01 mm thin quartz capillary (HILGENBERG) with diameter of 0.5 mm was glued in a 1/4'' VCR weld gland (SWAGELOK) and tested for a leak check up to 6 MPa with helium. After that the capillary was filled with the water-loaded silica and connected via a SWAGELOK thread to a pressure controller apparatus. All *in situ* experiments were carried out at the temperature of 243 K. The diffraction experiments were conducted in transmission geometry in the 2θ range from 5° to 90° using monochromatic synchrotron radiation

(E=8048 eV; λ = 1.5406 Å). The diffraction images from 2D detector were integrated using proprietary software. NIST silicon SRM 640a was used as external standard for peak positions. Before dosing methane, the pressure in the gas line was reduced to 50 kPa. The dosing of the methane was done in the pressure range between 0.05 and 6 MPa with 1 MPa steps. After 20 minutes of equilibration, the PXRD patterns were measured.

3. RESULTS AND DISCUSSION

3.1 Sample characterization

Nitrogen adsorption/desorption isotherms for the two selected ordered mesoporous silica, namely MCM – 41 and B – PMO, show a characteristic type IV shape according to the IUPAC classification,[37] typical for mesoporous structures with uniformed pore size (Fig.1a,c). The steep increase of the amount adsorbed at the relative pressures (p/p^0) around 0.3 is related to capillary condensation occurred within mesopores. No hysteresis loop is detected which indicates the same filling/emptying mechanism for these materials. The pore size distribution calculated by applying NLDFT to nitrogen data, assuming cylindrical pore shape, are very narrow and show a very similar pore size average for both samples, that is 4.4 nm for MCM - 41 and 3.8 nm for B – PMO (Fig.2b,d). Both BET area (S_{BET}) and total pore volume (V_p) at p/p^0~0.95 were also calculated from the nitrogen adsorption data. MCM – 41 shows values of S_{BET} = 925 m^2/g and V_p = 0.95 cm^3/g, whereas B – PMO shows a slightly inferior values of S_{BET} = 840 m^2/g and V_p = 0.74 cm^3/g. The low-angle x-ray diffraction pattern for B - PMO (Fig.1e) exhibits a main peak at 2θ = 1.96º ascribed to (100) and two weak reflections ascribed to (110) and (200) at 2θ = 3.4º and 3.9º, indicating hexagonally ordered pore structure. Similar pattern is revealed for MCM – 41 (Fig.1f).

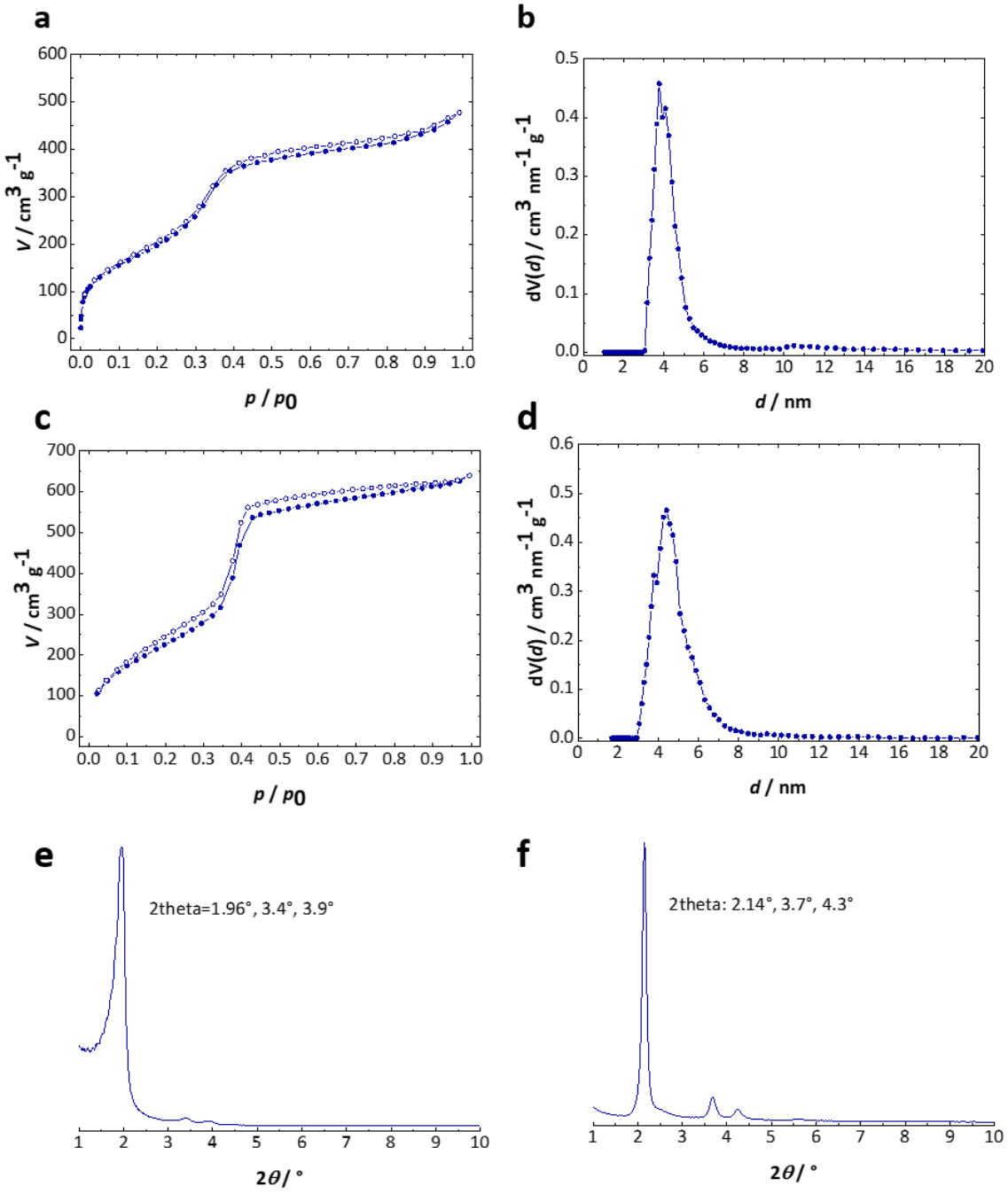


Figure 1. Nitrogen physisorption isotherm (77 K) of B – PMO (a) and MCM - 41. (c) The pore diameter distribution on the right (b) and (d) was calculated with NLDFT kernel from the adsorption branch for silica with cylindrical pores. Powder XRD pattern of B – PMO (e) and MCM - 41 (f) measured with STOE Stadi P (transmission geometry).

Water vapor adsorption/desorption experiments were conducted at 298 K and the resulting isotherms show a characteristic type V shape according to the IUPAC classification (Fig.2).[37] The

total water adsorption capacity is 32 mmol/g (0.58 cm^3/g, $\rho_{water} = 1\ cm^3/g$) for MCM – 41 and 27.8 mmol/g (0.50 cm^3/g, $\rho_{water} = 1\ cm^3/g$) for B - PMO at $p/p^0 \sim 0.95$. MCM – 41 exhibits a gradual rise in the water capacity up to 7.1 mmol/g at the onset of pore condensation ($p/p^0 \sim 0.54$). This value is considerable superior to that of 3.1 mmol/g showed by B – PMO at the onset of $p/p^0 \sim 0.55$, suggesting that MCM – 41 is more hydrophilic. Another observation is that the hysteresis loop (type H1) is narrower for B - PMO when comparing to MCM – 41. This might be due to a differences in the mean pore diameter (3.9 nm and 4.3 nm, respectively), although a different wettability might lead to a similar effect, that is the desorption requires significant lower relative pressures due to stronger interactions of the water molecules with the hydrophilic surface of MCM - 41 silica.[30,38] Mietner et al.[30] have reported that water only partially wets B – PMO due to the alternation between silanol and benzene groups on its surface, i.e. while the silanol groups has the ability to form hydrogen bonds, rendering the surface hydrophilic, the alternate distributions of benzene groups on the silica matrix leads to hydrophobic surface sites. Conversely, MCM – 41 exhibits merely silanol groups, being the absolute number of silanol groups much higher, resulting in a uniform surface wetting when exposed to water.

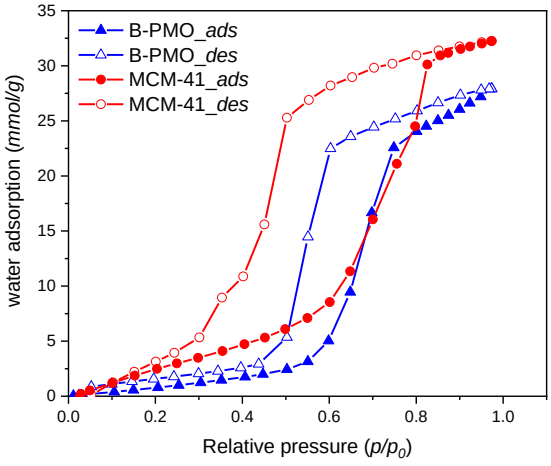


Figure 2. Water vapour adsorption (solid symbols) and desorption (empty symbols) isotherms for MCM – 41 (red circle) and B – PMO (blue triangle).

3.2 Water classification

Prior to methane hydrate formation, MCM – 41 and B – PMO were loaded with water to reach 80 % and 150 % of the total pore volume (V_p). That leads to unsaturated and oversaturated pores, respectively. Analyzing the water distribution in a given porous media is of paramount importance since the strong adsorption potential combining with hydrophilic pore walls extremely modifies the water activity, which in turns affect the methane hydrate stability.[39] Differential scanning calorimetry results (Fig.S1) confirm the depression in the melting and freezing point of water in the wetted samples respecting to bulk water, which is a clear demonstration of the confinement effect in mesopores and the reduction of the water activity.[28,40] To be precise, for samples loaded at 80%V_p, the heating profiles reveal a single endothermic peak at 234-235 K, corresponding to the melting point of ice in mesopores.[28,41] For B-PMO loaded with excess water up to reach 150%V_p, the heating profile reveal two endothermic peaks, the melting of confined ice around 234-235 K and the water on the external surface (outside the pore) that melts at 273 K as bulk water does (note, that this peak is absent in MCM-41 due to the high hydrophilicity of its surface)

Table 1 outlines the water distribution in MCM – 41 and B – PMO at the two selected water loadings in detail. Both, V_p (obtained from the nitrogen adsorption experiments) and total water adsorption capacity (obtained from the water vapor adsorption experiments) were considered to calculate the so-called core water and external water. We defined core water as the water that is located in mesopores but furthest from the pore wall, therefore a higher water activity is expected; whereas the external water is that located on the external surface without any geometrical constraints, i.e. bulk water. For example, sample MCM – 41 exhibits V_p = 0.95 cm^3/g_{silica}, and it is loaded with water up to reach 80% of the V_p, this is a water volume of

0.76 cm^3/g_{silica}; the water adsorption capacity is 0.58 cm^3/g_{silica}, therefore, the core water is calculated as 0.76 – 0.58 = 0.18 cm^3/g_{silica}. When sample MCM – 41 is loaded with water to reach 150% of the V_p, i.e. a water volume of 1.43 cm^3/g_{silica}, the core water is calculated as 0.95 – 0.58 = 0.37 cm^3/g_{silica}, the remaining water volume, 0.48 cm^3/g_{silica}, is the external water.

Table 1. Water distribution in wet MCM – 41 and B – PMO. Total pore volume calculated from nitrogen adsorption experiments and total water adsorption capacity extracted from water adsorption experiments are also included. The unit for all parameters is (cm^3/g_{silica}).

Sample	Total pore volume	Water loading	Water adsorption capacity	Core water	Free pore	External water
MCM-41_80%V_p	0.95	0.76	0.58	0.18	0.19	-
MCM-41_150%V_p	0.95	1.43	0.58	0.37 [a]	-	0.48
B-PMO_80%V_p	0.74	0.59	0.50	0.09	0.15	-
B-PMO_150%V_p	0.74	1.11	0.50	0.24 [a]	-	0.37

[a] *It is the total pore volume minus the water adsorption capacity.*

3.3 HP- methane sorption analysis

We conducted eighteen systematical high-pressure methane sorption experiments on MCM – 41 (Fig.3) and B – PMO (Fig.4) at three temperatures (275 K, 258 K and 243 K) before and after loading with water, namely 80% and 150% of total pore volume (V_p). For dry samples, the isotherms are type I according to IUPAC classification,[37] the maximal methane adsorption capacity tends to increase with decreasing temperature, as expected due to the exothermic nature of the adsorption phenomenon. The maximal methane adsorption capacity is 115 cm^3(STP)/g at 243 K and 6 MPa for MCM – 41, similar to other reported values in literature for this type of material.[27] B – PMO showed a lower value of 78.5 cm^3(STP)/g under same conditions, as expected due to its lower surface area. While dry samples have an inferior methane storage performance compared to materials like (HKUST - 1[42] and PPAC),[43] the amount of methane adsorbed is not negligible, indicating the high adsorption potential that pore walls exert in both materials. For wet samples the scenario changes dramatically, the shape of the isotherms changes and it strongly depends on the temperature, the pore loading and the studied sample (i.e. surface configuration). We therefore want to analyzed each case separately, before making a global

conclusion. For more information about the sorption experiments' set up, such as designed profile and equilibrium time, please, refer to section 3 in the ESI.

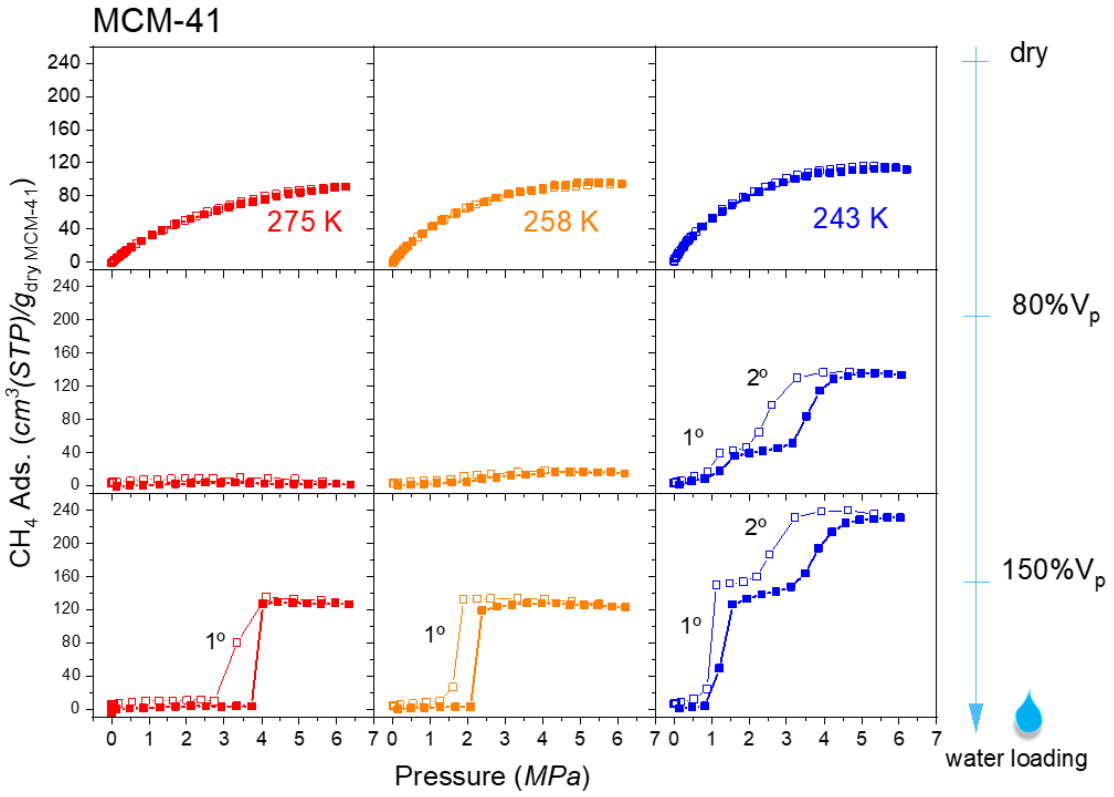


Figure 3. Methane adsorption (solid symbols) and desorption (empty symbols) isotherms at 243 K (blue), 258 K (orange) and 275 K (red) up to 6 MPa for dry MCM - 41 at two different water loadings 80%V_p and 150V_p, where V_p is the total pore volume. The y-axis refers to cm^3 (STP) of methane per g of dry silica. The numbers 1º and 2º point at the first and the second adsorption step with their associated hysteresis.

For MCM – 41 loaded with water at 80%V_p, the total methane uptake is practically nil in the full pressure range at 275 K (Table 2). The pre-adsorbed water molecules leave no place for methane molecules to be adsorbed on the surface. Moreover, the strong interaction between water molecules and silanol groups seems to prevent the formation of methane hydrate crystals under these conditions. Reducing the temperature to 258 K results in some methane uptake at the threshold pressure of 2 MPa. However, the highest value of 133 cm^3(STP)/$g_{dry\ MCM-41}$ is

achieved at 243 K, even surpassing its dry counterpart. The shape of the isotherm reveals that this amount of gas is consumed in two discrete steps (pointed out as 1º and 2º in Fig.3), each one associated to a hysteresis loop. In step 1º, there is a sudden rise in the methane capacity up to 42.6 $cm^3(STP)/g_{dry\ MCM-41}$ at 1.2 MPa, whereas in step 2º, an inflexion point occurs at the threshold pressure of 3.2 MPa, resulting in an extra gas consumption of 90.4 $cm^3(STP)/g_{dry\ MCM-41}$ (Table 2). Interestingly, when MCM – 41 is loaded with water at 150%V_p, at 275, 258 and 243 K, a sudden rise in the methane uptake is detected at the pressures of 3.7, 2.1 and 1.1 MPa, respectively. The methane uptake in this step is practically the same regardless of the temperature (~130 $cm^3(STP)/g_{dry\ MCM-41}$, Table 2). Once again at 243 K a second methane uptake step is detected leading to a total value of 231.2 $cm^3(STP)/g_{dry\ MCM-41}$, which is twofold the methane uptake capacity for dry MCM - 41. In conclusion, not only the methane uptake capacities but also the shape of the isotherms, suggest that a different phenomenon than merely physisorption is responsible for the methane consumption, most likely, methane hydrate formation.

The pressure-time change profile until equilibrium for MCM – 41 loading with water at 150%V_p at the three studied temperature were recorded and showed in ESI section 3, Fig.S2a-c. Results indicate that the kinetics for step 1º is fast and the equilibrium is reached in 1 h. Longer equilibrium times (around 6-12 h) are required for step 2º. The fast growth process of the step 1º is consistent with the rapidly formation of a solid thin film hydrate over bulk water. Further growth is limited due to the slow mass transfer throughout the film. When the temperature is low enough (i.e. 243 K), the energy barrier is overcome and more MH is formed at higher pressure in step 2º. Coming back to the isotherms data, the hysteresis associated to step 1º coincides to the conditions of MH dissociation reported for bulk water (see http://gashydrates.nist.gov/HydrateViewer/), while the hysteresis associated to step 2º closed at higher pressures, suggesting a different stability of MH crystals. Handa and Stupin[15] measured

the methane hydrate heat of dissociation in 7-nm-radius silica gel pores calorimetrically to be 45.92 kJ/mol, the corresponding value in bulk phase are 54.19 kJ/mol, i.e. confined hydrate is thermodynamically less stable. Additionally, kinetics recorded for step 1º reveal an induction time (nucleation periods), which is reduced when decreasing temperature (Table 2), whereas step 2º does not imply any induction time and the rate of pressure decay suggests a slow growing process of confined hydrate. Previous experiences[22] have shown that the induction time, and then the hysteresis 1º, can be eliminated in a second cycle due to the "memory effect".[44]

Table 2. Summary of experimental data extracted from sorption experiments for MCM - 41 and B - PMO, including, threshold pressures, induction time, total methane consumption at 6 MPa and total water-to-hydrate conversion.

Samples	T (K)	Threshold P (MPa)	Induction time (min)*	Total CH_4 consumed (cm^3(STP)/g_{silica})	Total CH_4 consumed (mol/mol of H_2O)	Total water-to-hydrate conversion (%)**
MCM-41_80%V_p	275	ND	ND	4	0.0013	0.8
	258	2.0	ND	16	0.0151	9.2
	243	1.2/3.2	84/ND	133	0.1406	85.8
MCM-41_150%V_p	275	3.7	285	127	0.0711	43.4
	258	2.1	200	128	0.0713	43.5
	243	1.1/3.3	40/ND	231	0.1302	79.4
B-PMO_80%V_p	275	5.3	ND	20	0.0272	16.6
	258	2.2	ND	40	0.0466	28.4
	243	1.1/3.7	ND	124.5	0.1689	103.0
B-PMO_150%V_p	275	5.3	985	38	0.0394	24.0
	258	2.1	210	130	0.1017	62.0
	243	0.9/3.7	0/ND	170	0.1306	79.7

HP-methane adsorption/desorption isotherms for B – PMO loaded with water at 80%V_p (Fig.4) show some striking differences comparing to MCM – 41. Although low, at 275 K some methane consumption can be detected at the threshold pressure of 5.3 MPa (Table 2). The methane uptake slightly increases at 258 K and 2.2 MPa. At the lowest temperature of 243 K the methane consumption occurs in two discrete steps, at threshold pressure of 1.1 MPa (1º) and 3.7 MPa (2º), giving rise to a total methane uptake of 124.5 cm^3(STP)/$g_{dry\ B\ -\ PMO}$. For B – PMO loading with water at 150%V_p, the threshold pressure is not defined at 275 K and 258 K which suggests that both, adsorption and MH formation may contribute simultaneously to the methane consumption rate. Taking into account the alternation of the benzene and silanol groups on the surface of B –

PMO, it seems reasonable for methane molecules being strongly adsorbed by the organic group. Finally, at the lowest temperature of 243 K the methane consumption occurs in two discrete steps, a steep jump at 0.9 MPa (1º) and at threshold pressure of 3.7 MPa (2º), giving rise to a highest total methane uptake of 170 $cm^3(STP)/g_{dry\ B\ -\ PMO}$. Similar behavior was observed for carbon materials in previous reports.[18,25,45] An interesting observation is that the desorption branches do not reach zero, which means that some methane molecules remain trapped in the system either adsorbed or in hydrate form (Table 3). The pressure-time change profile until equilibrium for B – PMO loading with water at 150%V_p at the three studied temperature were recorded and showed in ESI section 3, Fig.S2d-f. Results indicate that the growing kinetics for step 1º is slower than that for MCM – 41 and the equilibrium is reached in 6 h. Similar tendency

were found between hydrophobic and hydrophilic ordered mesoporous carbon in previous studies.[18]

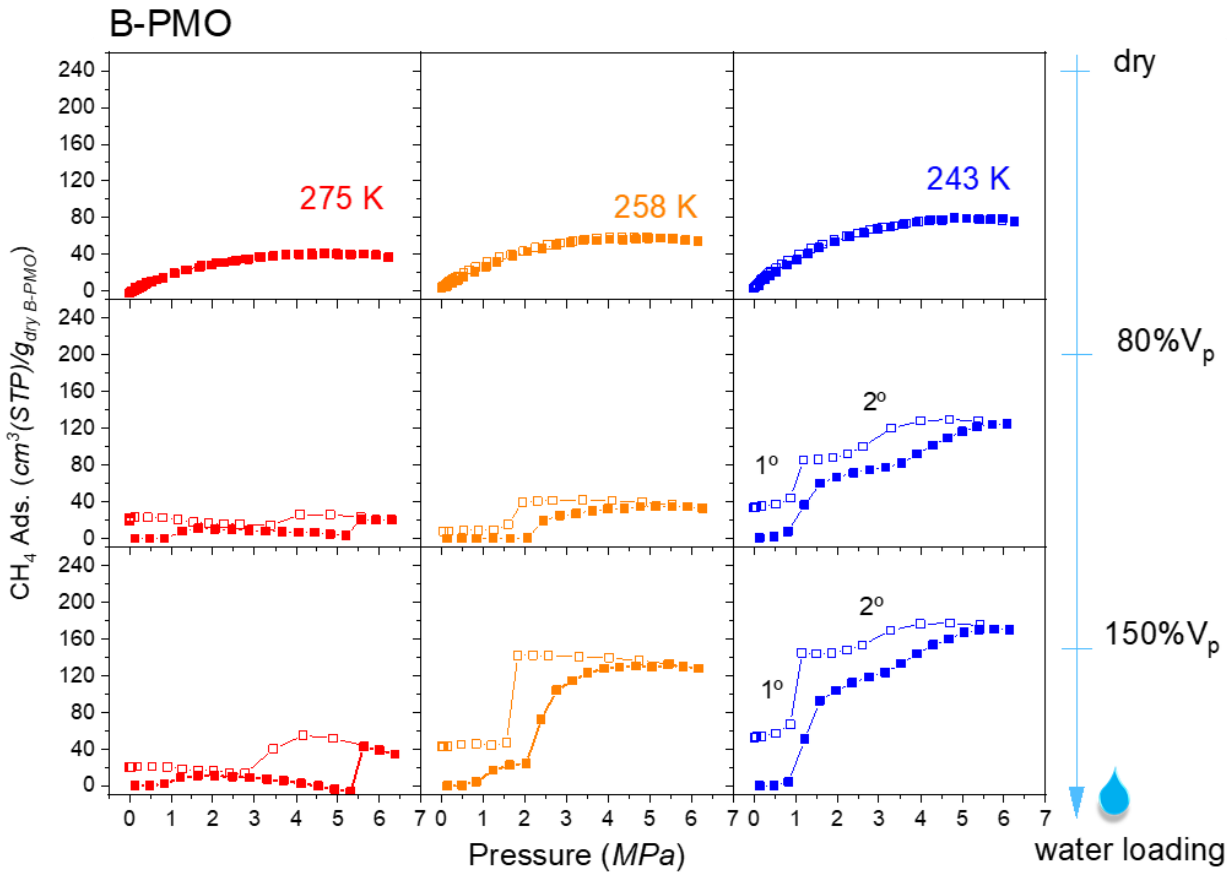


Figure 4. Methane adsorption (solid symbols) and desorption (empty symbols) isotherms at 243 K (blue), 258 K (orange) and 275 K (red) up to 6 MPa for dry B – PMO at two different water loadings 80%V_p and 150V_p, where V_p is the total pore volume. The y-axis refers to cm^3 (STP) of methane per g of dry silica. The numbers 1º and 2º point at the first and the second adsorption step with their associated hysteresis.

Table 3. Methane uptake and released extracted from the first (1º) and second (2º) step of the sorption experiments for MCM - 41 and B - PMO at 243 K. The unit for all parameters is $cm^3(STP)/g_{silica}$.

Sample	CH_4 uptake 1º	CH_4 uptake 2º	CH_4 released 1º	CH_4 released 2º	CH_4 trapped [a]
MCM-41_dry	115	-	115	-	0
MCM-41_80%V_p	42.6	90.4	42.6	90.4	0
MCM-41_150%V_p	126.4	104.8	150.1	81.1	0
B-PMO_dry	78.5	-	78.5	-	0
B-PMO_80%V_p	59.6	64.9	52.3	42.5	33
B-PMO_150%V_p	92.3	77.7	92.2	32.4	52.6

[a] *The desorption branch does not reach zero. This indicates that some amount of methane remains trapped in the system.*

Several publications have reported that a higher driving force results in a rougher hydrate film,[46] which means a more chaotic polycrystalline MH phase, as consequence, an increase in the mass transfer throughout the grain boundary is expected.[47] If it is assumed that adsorbed water remains in mesopores while the core and external water forms the above mentioned rough hydrate film, therefore, two opposites possibilities emerge: either methane molecules diffuse through the hydrate layer toward the inner porosity, or alternatively, water may diffuse toward the outer surface to perpetuate MH growth. Both possibilities consume methane. Siangsai et al.[48] observed two steps methane consumption in a unstirred reactor loaded with wet activated carbons. Jin et al.[49] attributed this phenomenon to the collapse of the film-like hydrate following by the mass transfer of fresh water molecules into the hydrate phase, changing from film-like to cement-like hydrate. In our experiments the answer could be found looking at the desorption branch in Fig.3 and Fig.4. The observed hysteresis in step 2º closes around 2.2 MPa in all cases, that is a shift of 1.4 MPa respecting the equilibrium condition for MH dissociation, which means that methane consumption is not linked to MH formation on the outer surface, i.e. bulk MHs could be ruled out. Conversely, methane molecules might diffuse throughout the rough thin film to meet confined water. A combination of high adsorption potential and high methane pressure at 243 K might offer the necessary driving force to overcome the mass transfer limitations increasing the methane gas saturation in water, and, therefore promoting confined hydrate nucleation and growth.

Jacobson et al.[50] proposed the 'blob mechanism' for MH crystallization in water rich methane gas, which involves a first reversible step of formation of aggregates of guests separated by water molecules (the blobs). If the blob is sufficiently large and long-lived (a radius of around 1 nm at 240 K),[51] the water molecules surrounding the solvent-separated guests form persistent polyhedral cages resulting in an amorphous clathrate intermediate that can ripe to the crystalline

clathrate phase. Jacobson et al.[51] also demonstrated that the temperature dependence of the critical nucleus size (R) is well described by the Gibbs-Thomson relation, being R ~1 nm and 1.5 nm for crystalline and amorphous nuclei, respectively at 243 K. Solely sorption experiments do not provide enough experimental evidence for the existence nanohydrates of size below 4 nm in silica mesopores. Nevertheless, results suggest that the interaction between methane and water in mesopores is strong enough to enhance the methane capacity from step 1º to step 2º by 50%. Comparing to dry materials where merely physisorption occurs, the extra formation of MHs improves the uptake around 50%, demonstrating the advantages of wetting both studied silica in a hypothetical methane storage system.[25]

3.4 Water behavior during hydrate formation

The water behavior during methane hydrate formation process at 243 K in MCM – 41 and B – PMO were investigated from the adsorption experiments. Fig.5 shows a bar graph correlating the water volume of the different types of water in pores: (1) before methane uptake as was described in section 3.2, (2) after methane uptake, that is the water involved in MH formation in step 1º and 2º, and (3) after methane release, that is the water released during MH dissociation in step 1º and 2º. In order to calculate the water volume involved in the MH formation/dissociation processes in steps 1º and 2º, the amount of methane uptake and released listed in Table 3 is used, assuming that MH structure I is formed indistinctively in both steps.[52] Hydration numbers between 5.8 to 6.3 (depending on the cage occupancy factor) were reported in literature for artificial and natural occurring MH,[53–55] here we selected 6.1 for all calculations.

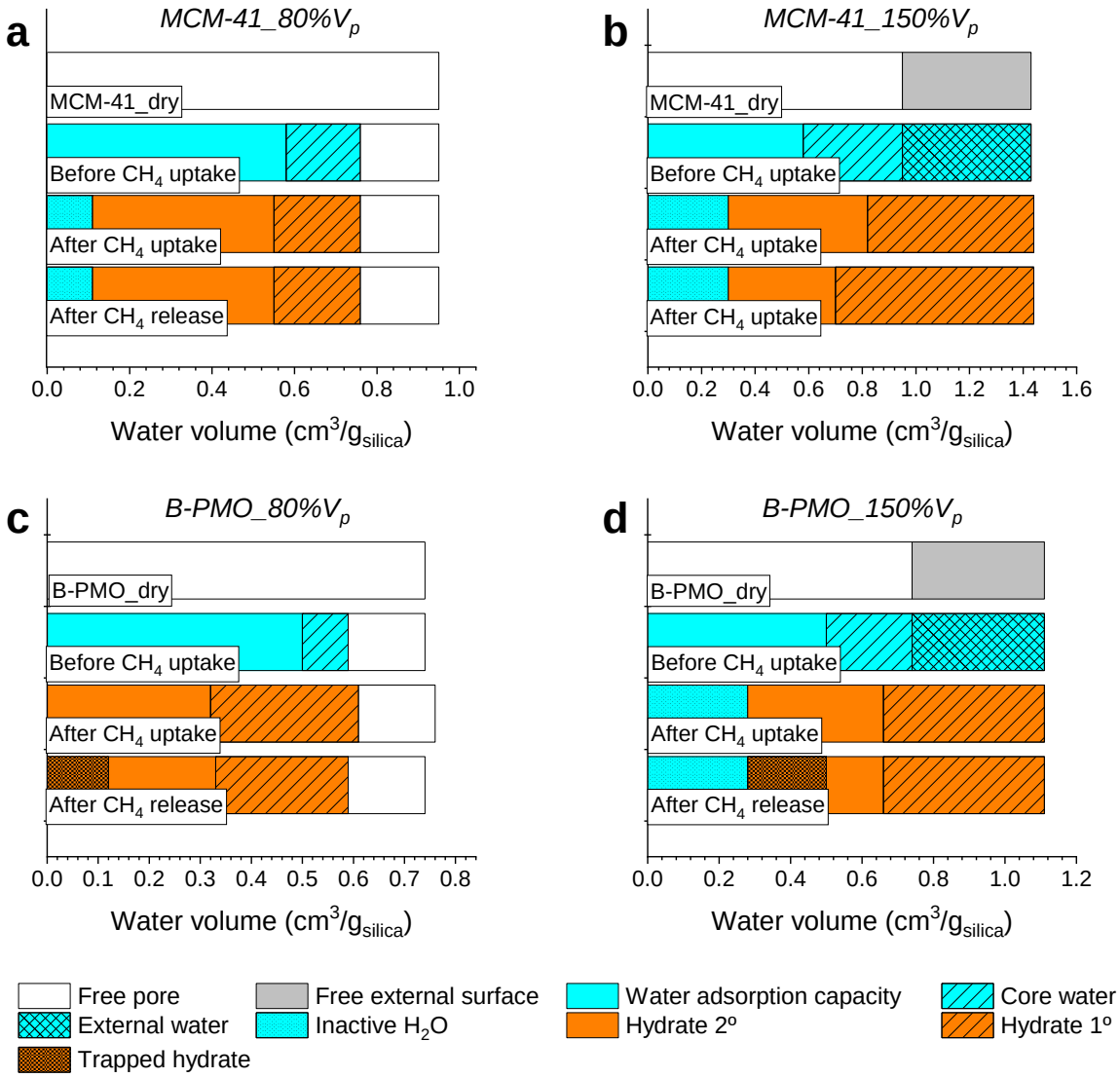


Figure 5. Bar graph showing the water volume in pores before methane uptake, after methane uptake and after methane release at 243K for **a** MCM - 41_80%V_p, **b** MCM - 41_150%V_p, **c** B - PMO_80%V_p and **d** B - PMO_150%V_p, where V_p is the total pore volume. The water volume involves in MH formation during steps 1º and 2º detected in the adsorption branch of the isotherms and the water volume involves in MH dissociation during steps 1º and 2º detected in the desorption branch of the isotherms were calculated assuming hydration number of 6.1. This type of water is identified as ´hydrate 1º´ and ´hydrate 2º` in the graphs. Note that for B-PMO there is water forming MH even after methane release.

Comparing the water volume before and after methane uptake for MCM – 41_80%V_p (Fig.5a), suggests that the core water in mesopores forms MH in step 1º. As was explained in section 3.2, this type of water is not bounded to the pore walls and it is less attracted by the pore potential, being considered rather as 'free water' able to be converted to MH. The core water in mesopores

is uniformly distributed along the silica surface forming a water thin film rich in methane gas which promotes the nucleation and a fast growing of film-like MHs. Once these structures are formed, excess methane must diffuse throughout the crystals boundary network to reach the adsorbed water.[47] Our calculations indicate that 19 % of this water (14.4 % of the total water in the system) is not prone to participate in MH formation and must be assigned to the non-freezable water at the hydrophilic pore wall (around 2-3 monolayer of water, 0.4-0.8 nm).[56] In Fig.5 it is identified as inactive water. The remaining water is the so-called freezable water and it is able to meet methane gas to form confined hydrate in step 2º. Finally, the water volume before and after methane release in steps 1º and 2º perfectly match indicating the reversibility of the whole process. For sample MCM – 41_150%V_p the situation is quite similar with the exception that there is water outside the pore, which it is identified in Fig.5 as external water. In this case, this water promotes the formation of MH on the external surface and seems to drag certain proportion of the core water during MH crystallization in step 1º. The remaining core water and some proportion of adsorbed water form MH during step 2º. A percentage of 51.7 % of the adsorbed water in mesopores (20% of the total water in the system) is not prone to form MH. In conclusion, the water behavior during the MH formation/dissociation processes is linked to the following water activity trend as the molecules move away from the pore wall: bulk water~external water > core water> freezable water> non-freezable water.

For sample B – PMO _80%V_p, results are quite different. In this case, both the core water and certain proportion of adsorbed water form MHs during step 1º. During step 2º the remaining adsorbed water in mesopores is fully converted to MH, which means that even the water molecules at the silica surface is prone to nucleate, suggesting higher water activity than in the case of MCM – 41. The explanation lies in the surface configurations of B – PMO. The organic groups adsorb methane gas that saturates and displace the adsorbed water in mesopores further

from the wall, i.e. the water has more mobility in B – PMO than in MCM – 41, promoting the nucleation and growth of MH crystals on this interface. Similar results were reported for hydrophobic ordered mesoporous carbon.[18] Surprisingly, our calculations suggest that while water volume involved in MH formation in step 1º is fully recovered, some proportion of water volume involved in MH formation during step 2º remains trapped as MH even after methane depressurization. This also happen in sample B – PMO_150%V_p. This apparent hydrate stability is called 'self-preservation effect'.[57] After the initial hydrate dissociation into ice and gas, the hydrate became totally encapsulated by the pore walls and the ice caps at 243 K. The hydrates trapped in the interior of the pore remained stable up to the melting point of ice.[15] A small quantity around 8 cm^3(STP)/g of methane gas remains adsorbed in B – PMO regardless of the water loading (see calculus in ESI section 4). In B – PMO_150%V_p, the water volume behavior is similar to the latter case, excepted for the existence of external water and a high percentage of inactive water (20.3% of the total water in the system). From the analysis, we can anticipate that the inactive water is rather inactive bulk ice as we will confirm in the following section.

3.5 Synchrotron powder x-ray diffraction

In situ powder X-ray diffraction (SPXRD) patters for MCM – 41 and B – PMO with water loading of 150%V_p were measured at the BESSY synchrotron facility (for details see ESI section 5). The methane pressure was increased stepwise from 1 to 6 MPa at 243 K (Fig.6). Both MCM – 41 and B – PMO show the pattern of the hexagonal structure of ice due to the water molecules outside the pore, in agreement with DSC results (Fig.S1). When the system reaches 2 MPa of methane pressure, the characteristic peaks of methane hydrate crystals structure I are revealed in both cases. For MCM – 41 ice peaks completely disappear, whereas for B – PMO, ice peaks still prevail even at 6 MPa. This observation proofs that the inactive water in B – PMO corresponds to bulk ice instead of non-freezable water.

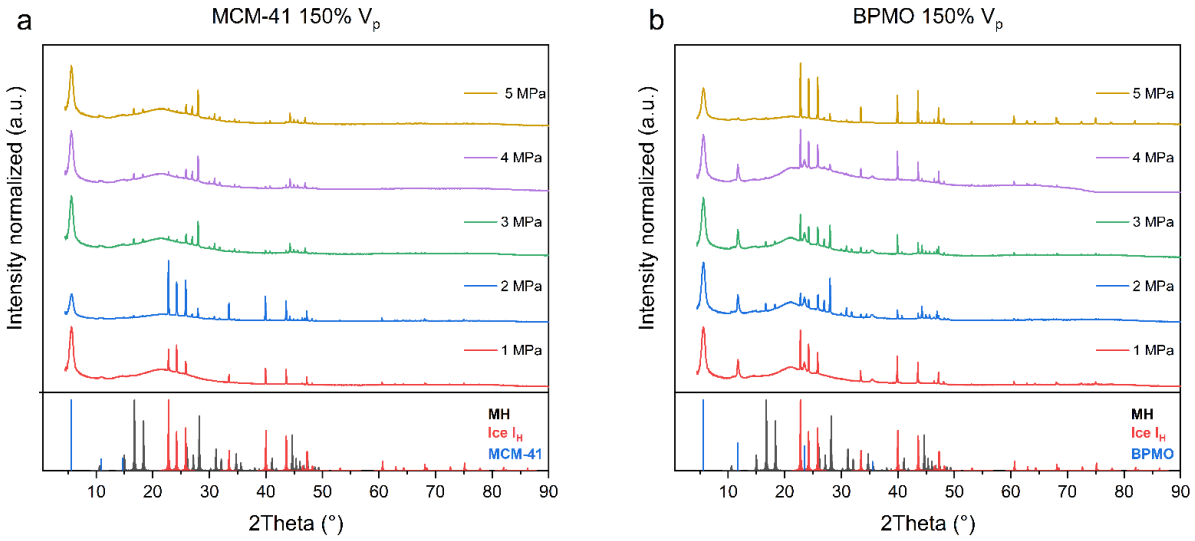


Figure 6. In situ synchrotron X-ray powder diffraction patterns for **a** MCM - 41 and **b** B- PMO at the water loading of 150%V_p, where V_p is the total pore volume.

Finally, in Fig.7 we propose a model showing how the water behaves before methane uptake, after methane uptake and after methane release taking into consideration all the information collected from Figure 5, SPXRD, DSC and the surface configuration of the studied silica. On the left and right panel, mesopores of MCM – 41 and B – PMO loaded with water to reach 150% of the total pore volume are shown, respectively. The samples are cooled down to 243 K before pressurizing with methane, under this condition different type of water can be observed: external water (solid), core water (solid) and adsorbed water. During methane pressurization, the surface of MCM – 41 are completely blocked by non-freezable water while the surface of the B – PMO has free space for methane to be adsorbed. After methane uptake two types of hydrates were formed in two discrete steps: bulk hydrate in step 1º and confined hydrate in step 2º. Additionally, there is water that cannot be converted to hydrate in both silica, for MCM – 41 this water is the non-freezable water at the pore wall, whereas for B – PMO, this water is ice located on the external surface (detectable by SPXRD), likely in the interior of large ice clusters where methane cannot diffuse. After depressurization, the methane gas is released from the MH

crystals. In the case of MCM – 41 the process is fully reversible. However, for B – PMO some of the confined hydrate and free methane remained trapped on the mesopores walls. Extended version of Fig.7 is illustrated in ESI section 4.

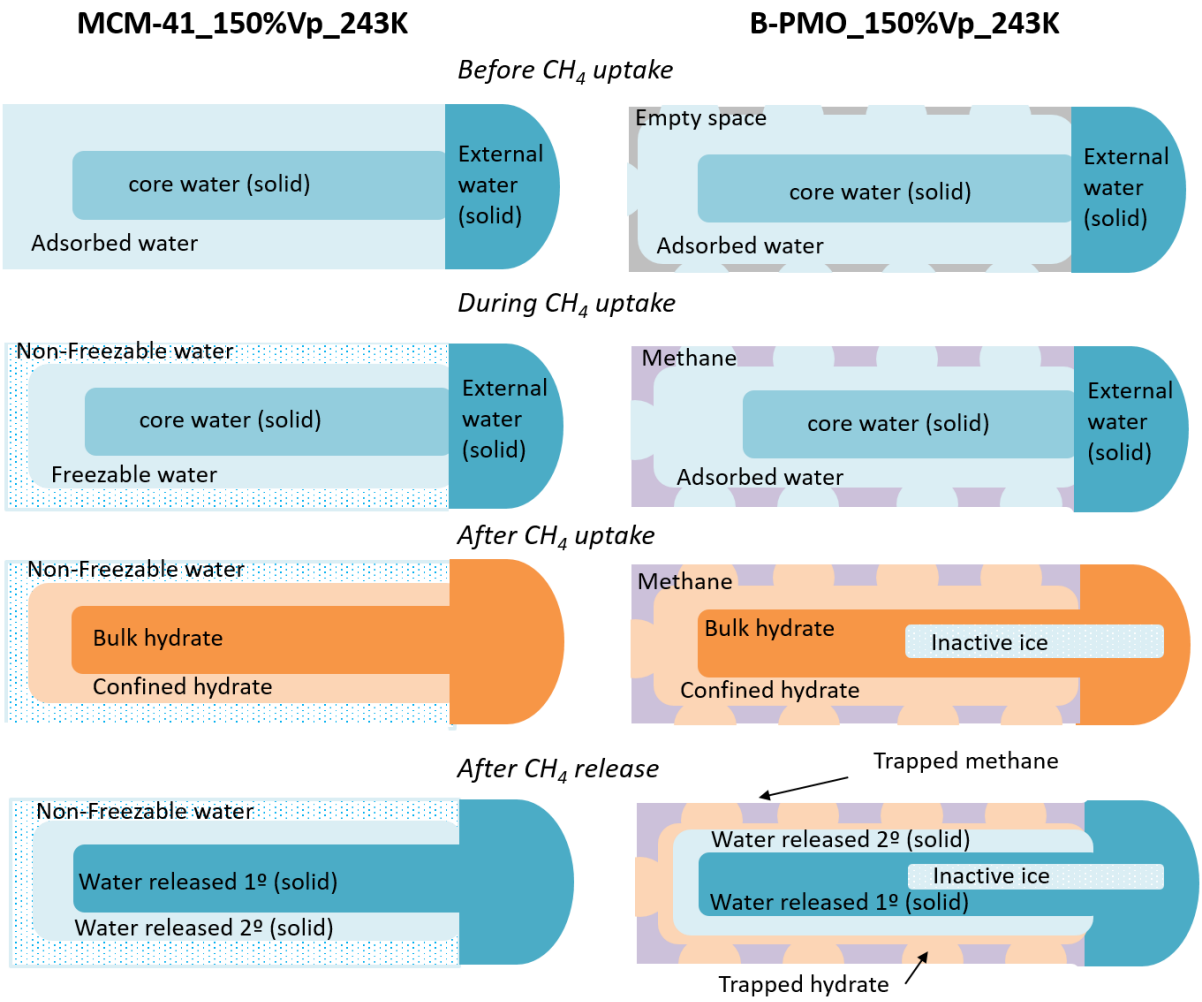


Figure 7. Mechanistic model of methane hydrate formation in MCM – 41 and B – PMO loaded with water up to reach 150% of the total pore volume at 243 K. The different shades of blue illustrate different types of water. Gray color represents the empty space. Dark orange represents bulk hydrate formed in step 1º, whereas light orange represents confined hydrate formed in step 2º. Lilac color represents methane in gas phase. Note non-freezable water at the pore wall in MCM - 41 and inactive ice in B – PMO.

4. CONCLUSION

We have used HP- methane adsorption/desorption isotherms to study the methane hydrate formation process in the pore space of MCM – 41 and benzene - PMO with highly ordered pore structure and well-defined surface configuration. Results showed that methane is taken up in two discrete steps (labeled 1º and 2º) at 243 K in both samples and at the two studied water loading, 80% and 150% of V_p. Methane consumption in step 1º is ascribed to the formation of bulk hydrate consuming external and core water; and methane consumption in step 2º is ascribed to the formation of less stable confined hydrate crystals with the adsorbed water in mesopores. The different wettability between samples exert an important influence in the nucleation and growth mechanisms in mesopores. MCM – 41 exhibits uniform wettability forming a thin film over the surface that rapidly form MHs crystals, however, the hydrophilic surface renders non-freezable water at the pore wall not prone to form MH. In the case of B – PMO the alternate arrangement of the water on the surface offers free area for methane molecules to be adsorbed and displace the water far from the pore wall to form MHs. PXRD results reveal that inactive ice is present on the outer surface co-existing with MHs crystals in B – PMO while ice in MCM – 41 is fully converted to hydrate. After depressurization a small quantity of methane gas remained trapped in adsorbed and in hydrate form within the mesopores of B – PMO. We finally proposed a model to illustrate the different types of water and hydrates in pores before and after pressurizing with methane gas.

Appendix A. Supporting information

Acknowledgement

MEC acknowledges the Alexander von Humboldt foundation and Agencia Nacional de Investigación e Innovación (PD_NAC_2018_1_150145) for financial support. LB, SG gratefully acknowledge the Federal Ministry of Education and Research (Bundesministerium für Bildung

und Forschung, BMBF) for support of the Mechanocarb project (award number 03SF0498), LB thanks Daimler und Benz-Stiftung (award number 32-01/16). All the authors thank the Helmholtz-Zentrum Berlin for financial support and allocation of synchrotron radiation beam time at the KMC-2 beamline.

Authors contributions

MB and NS synthesized and characterized the PMO and MCM-41 silica materials (supervision by MF), respectively. MEC performed the methane adsorption experiment. MEC and LB conducted and interpreted experiments. SG, DW, NG, DM conducted the *in situ* PXRD investigations. Among these authors DM was the responsible of beam line at BESSY II. MEC wrote the manuscript. All the authors critically revised and approved the manuscript.

Competing finance interests

The authors declare that they have no known competing financial interests or personal relationships that could have appeared to influence the work reported in this paper.

REFERENCES

1 G. C. K. Leung, Natural Gas as a Clean Fuel, Handb. Clean Energy Syst. (2015) 1–15. https://doi.org/10.1002/9781118991978.hces055

2 K. A. Kvenvolden, Methane hydrate — A major reservoir of carbon in the shallow geosphere?, Chem. Geol. 71 (1988) 41–51. https://doi.org/10.1016/0009-2541(88)90104-0

3 C. Ruppel, Permafrost-associated gas hydrate: Is it really approximately 1 % of the global system?, J. Chem. Eng. Data. 60 (2015) 429–436. https://doi.org/10.1021/je500770m

4 G. Rehder, R. Eckl, M. Elfgen, A. Falenty, R. Hamann, N. Kähler, W. F. Kuhs, H. Osterkamp and C. Windmeier, Methane hydrate pellet transport using the self-preservation effect:

A techno-economic analysis, Energies. 5 (2012) 2499–2523. https://doi.org/10.3390/en5072499

5 H. Mimachi, M. Takahashi, S. Takeya, Y. Gotoh, A. Yoneyama, K. Hyodo, T. Takeda and T. Murayama, Effect of Long-Term Storage and Thermal History on the Gas Content of Natural Gas Hydrate Pellets under Ambient Pressure, Energy & Fuels. 29 (2015) 4827–4834. https://doi.org/10.1021/acs.energyfuels.5b00832

6 E. Dendy Sloan, C. A. Koh. Clathrate hydrates of natural gases, third ed., CRC Press, Taylor and Francis group, Boca Ratón, 2007.

7 H. P. Veluswamy, A. Kumar, Y. Seo, J. D. Lee and P. Linga, A review of solidified natural gas (SNG) technology for gas storage via clathrate hydrates, Appl. Energy. 216 (2018) 262–285. https://doi.org/10.1016/j.apenergy.2018.02.059

8 L. Borchardt, W. Nickel, M. E. Casco, I. Senkovska, V. Bon, D. Wallacher, N. Grimm, S. Krause, J. Silvestre-Albero, D. Wallacher, N. Grimm, S. Krause and J. J. Silvestre-Albero, Illuminating solid gas storage in confined spaces - methane hydrate formation in porous model carbons, Phys. Chem. Chem. Phys. 18 (2016) 20607–20614. https://doi.org/10.1039/C6CP03993F

9 Z. R. Chong, S. H. B. Yang, P. Babu, P. Linga and X. Sen Li, Review of natural gas hydrates as an energy resource: Prospects and challenges, Appl. Energy. 162 (2016) 1633–1652. https://doi.org/10.1016/j.apenergy.2014.12.061

10 M. Khurana, Z. Yin and P. Linga, A review of clathrate hydrate nucleation, ACS Sustain. Chem. Eng. 5 (2017) 11176–11203. https://doi.org/10.1021/acssuschemeng.7b03238

11 X. Lang, S. Fan and Y. Wang, Intensification of methane and hydrogen storage in clathrate hydrate and future prospect, J. Nat. Gas Chem. 19 (2010) 203–209. https://doi.org/10.1016/S1003-9953(09)60079-7

12 C. Cuadrado-Collados, J. Farrando-Pérez, M. Martínez-Escandell, A. Missyul and J. Silvestre-Albero, Effect of additives in the nucleation and growth of methane hydrates confined in a high-surface area activated carbon material, Chem. Eng. J. 388 (2020) 124224.

https://doi.org/10.1016/j.cej.2020.124224

13 N. Kalogerakis, U. Calgary, A. K. M. Jamaluddin and N. T. Centre, Effect of Surfactants on Hydrate Formation Kinetics. Society of Petroleum Engineers. SPE International Symposium on Oilfield Chemistry 1993. https://doi.org/10.2118/25188-MS

14 B. Lucia, B. Castellani, F. Rossi, F. Cotana, E. Morini, A. Nicolini and M. Filipponi, Experimental investigations on scaled-up methane hydrate production with surfactant promotion: Energy considerations, J. Pet. Sci. Eng. 120 (2014) 187–193. https://doi.org/10.1016/j.petrol.2014.06.015

15 Y. P. Handa and D. Stupin, Thermodynamic properties and dissociation characteristics of methane and propane hydrates in 70-angstrom-radius silica-gel pores, J. Phys. Chem. 96, 21 (1992) 8599–8603. https://doi.org/10.1021/j100200a071

16 P. Linga, C. Haligva, S. C. Nam, J. A. Ripmeester and P. Englezos, Gas hydrate formation in a variable volume bed of silica sand particles, Energy & Fuels. 23 (2009) 5496–5507. https://doi.org/10.1021/ef900542m

17 A. Perrin, A. Celzard, J. F. Marěché, G. Furdin, Methane storage within dry and wet active carbons: A comparative study, Energy and Fuels.17, 5 (2003) 1283 – 1291. https://doi.org/10.1021/ef030067i

18 M. E. Casco, E. Zhang, S. Grätz, S. Krause, V. Bon, D. Wallacher, N. Grimm, D. M. Többens, T. Hauß and L. Borchardt, Experimental Evidence of Confined Methane Hydrate in Hydrophilic and Hydrophobic Model Carbons, J. Phys. Chem. C, 123 (2019) 24071–24079. https://doi.org/10.1021/acs.jpcc.9b06366

19 W. Wang, C. L. Bray, D. J. Adams and A. I. Cooper, Methane storage in dry water gas hydrates, J. Am. Chem. Soc. 130 (2008) 11608–11609. https://doi.org/10.1021/ja8048173

20 E. Andres-Garcia, A. Dikhtiarenko, F. Fauth, J. Silvestre-Albero, E. V. Ramos-Fernández, J. Gascon, A. Corma and F. Kapteijn, Methane hydrates: Nucleation in microporous materials, Chem. Eng. J. 360 (2019) 569–576. https://doi.org/10.1016/j.cej.2018.11.216

21 P. S. R. Prasad, Methane hydrate formation and dissociation in the presence of hollow silica, J. Chem. Eng. Data, 60 (2014) 304–310. https://doi.org/10.1021/je500597r

22 M. E. Casco, F. Rey, J. L. Jordá, S. Rudić, F. Fauth, M. Martínez-Escandell, F. Rodríguez-Reinoso, E. V. Ramos-Fernández, J. Silvestre-Albero, S. Rudic, F. Fauth, M. Martínez-Escandell, F. Rodríguez-Reinoso, E. V. Ramos-Fernández and J. Silvestre-Albero, Paving the way for methane hydrate formation on metal–organic frameworks (MOFs), Chem. Sci. 7 (2016) 3658-3666. https://doi.org/10.1039/C6SC00272B

23 C. Cuadrado-Collados, G. Mouchaham, L. Daemen, Y. Cheng, A. Ramirez-Cuesta, H. Aggarwal, A. Missyul, M. Eddaoudi, Y. Belmabkhout and J. Silvestre-Albero, Quest for an Optimal Methane Hydrate Formation in the Pores of Hydrolytically Stable Metal–Organic Frameworks, J. Am. Chem. Soc. (2020). https://doi.org/10.1021/jacs.0c01459

24 K. S. V, G. Udayabhanu, A. Mandal and S. Laik, Methane Hydrate Formation and Dissociation in the Presence of Silica Sand and Bentonite Clay, Oil Gas Sci. Technol. 70 (2015) 1087- 1099. https://doi.org/10.2516/ogst/2013200

25 M. E. Casco, J. Silvestre-Albero, A. J. Ramírez-Cuesta, F. Rey, J. L. Jordá, A. Urakawa, I. Peral, M. Martínez-Escandell, K. Kaneko, F. Rodríguez-Reinoso, Methane hydrate formation in confined nanospace can surpass nature, Nat. Commun. 6 (2015) 6432. http://www.nature.com/doifinder/10.1038/ncomms7432

26 C. Cuadrado-Collados, A. A. A. Majid, M. Martínez-Escandell, L. L. Daemen, A. Missyul, C. Koh, J. Silvestre-Albero, Freezing/melting of water in the confined nanospace of carbon materials: Effect of an external stimulus, Carbon N. Y. 158 (2020) 346–355. https://doi.org/10.1016/j.carbon.2019.10.081

27 X. Liu, D. Liu, W. Xie, X. Cui and Y. Chen, Methane Hydrate Uptake of MCM-41 Mesoporous Molecular Sieves with Preadsorbed Water, J. Chem. Eng. Data, 63 (2018) 1767–1772. https://doi.org/10.1021/acs.jced.8b00060

28 A. Schreiber, I. Ketelsen and G. H. Findenegg, Melting and freezing of water in ordered

mesoporous silica materials, Phys. Chem. Chem. Phys. 3 (2001) 1185–1195. https://doi.org/10.1039/B010086M

29 C. Faivre, D. Bellet and G. Dolino, Phase transitions of fluids confined in porous silicon: A differential calorimetry investigation, Eur. Phys. J. B. 7 (1999) 19–36. https://doi.org/10.1007/s100510050586

30 J. B. Mietner, F. J. Brieler, Y. J. Lee and M. Fröba, Properties of Water Confined in Periodic Mesoporous Organosilicas: Nanoimprinting the Local Structure, Angew. Chemie - Int. Ed., 56 (2017) 12348–12351. https://doi.org/10.1002/anie.201705707

31 M. C. Burleigh, S. Jayasundera, C. W. Thomas, M. S. Spector, M. A. Markowitz and B. P. Gaber, A versatile synthetic approach to periodic mesoporous organosilicas, Colloid Polym. Sci. 282 (2004) 728–733. https://doi.org/10.1007/s00396-003-1004-0

32 M. J. MacLachlan, T. Asefa and G. A. Ozin, Writing on the Wall with a New Synthetic Quill, Chem. – A Eur. J. 6 (2000) 2507–2511. https://doi.org/10.1002/1521-3765(20000717)6:14<2507::AID-CHEM2507>3.0.CO;2-9

33 W. Lin, Q. Cai, W. Pang, Y. Yue and B. Zou, New mineralization agents for the synthesis of MCM-41, Microporous Mesoporous Mater. 33 (1999) 187–196. https://doi.org/10.1016/S1387-1811(99)00137-7

34 K. J. Shea, D. A. Loy and O. Webster, Arylsilsesquioxane Gels and Related Materials. New Hybrids of Organic and Inorganic Networks, J. Am. Chem. Soc. 114 (1992) 6700–6710. https://doi.org/10.1021/ja00043a014

35 J. Landers, G. Y. Gor and A. V. Neimark, Density functional theory methods for characterization of porous materials, Colloids Surfaces A Physicochem. Eng. Asp. 437 (2013) 3–32. https://doi.org/10.1016/j.colsurfa.2013.01.007

36 S. Brunauer, P. H. Emmett and E. Teller, Adsorption of gases in multimolecular layers, *J.* Am. Chem. Soc. 60 (1938) 309–319. https://doi.org/10.1021/ja01269a023

37 M. Thommes, K. Kaneko, A. V Neimark, J. P. Olivier, F. Rodriguez-Reinoso, J. Rouquerol and K. S. W. Sing, IUPAC Technical Report Physisorption of gases, with special reference to the evaluation of surface area and pore size distribution (IUPAC Technical Report), Pure Appl. Chem. 87 (2015) 1051–1069. https://doi.org/10.1515/pac-2014-1117

38 M. Thommes, J. Morell, K. A. Cychosz and M. Fröba, Combining Nitrogen, Argon, and Water Adsorption for Advanced Characterization of Ordered Mesoporous Carbons (CMKs) and Periodic Mesoporous Organosilicas (PMOs), Langmuir. 29 (2013) 14893–14902. https://doi.org/10.1021/la402832b

39 T. Uchida, T. Ebinuma and T. Ishizaki, Dissociation Condition Measurements of Methane Hydrate in Confined Small Pores of Porous Glass, J. Phys. Chem. B. 103 (1999) 3659–3662. https://doi.org/10.1021/jp984559l

40 G. K. Rennie and J. Clifford, Melting of ice in porous solids, J. Chem. Soc. Faraday Trans. 1 Phys. Chem. Condens. Phases. 73 (1977) 680–689. https://doi.org/10.1039/F19777300680

41 G. H. Findenegg, S. Jähnert, D. Akcakayiran and A. Schreiber, Freezing and melting of water confined in silica nanopores, WILEY-VCH Verlag, 2008, vol. 9.

42 T. Tian, Z. Zeng, D. Vulpe, M. E. Casco, G. Divitini, P. A. Midgley, J. Silvestre-Albero, J.-C. Tan, P. Z. Moghadam and D. Fairen-Jimenez, A sol-gel monolithic metal-organic framework with enhanced methane uptake, Nat. Mater.17 (2018) 174-179. https://doi.org/10.1038/nmat5050

43 M. E. Casco, M. Martínez-Escandell, K. Kaneko, J. Silvestre-Albero and F. Rodríguez-Reinoso, Very high methane uptake on activated carbons prepared from mesophase pitch: A compromise between microporosity and bulk density, Carbon. 93 (2015) 693-701. https://doi.org/10.1016/j.carbon.2015.05.029

44 P. Buchanan, A. K. Soper, H. Thompson, R. E. Westacott, J. L. Creek, G. Hobson and C. A. Koh, Search for memory effects in methane hydrate: Structure of water before hydrate formation and after hydrate decomposition, J. Chem. Phys. 123 (2005) 164507. https://doi.org/10.1063/1.2074927

45 M. E. Casco, C. Cuadrado-Collados, M. Martínez-Escandell, F. Rodríguez-Reinoso and J. Silvestre-Albero, Influence of the oxygen-containing surface functional groups in the methane hydrate nucleation and growth in nanoporous carbon, Carbon. 123 (2017) 299–301. https://doi.org/10.1016/j.carbon.2017.07.061

46 H. Sharifi and P. Englezos, Accelerated hydrate crystal growth in the presence of low dosage additives known as kinetic hydrate inhibitors, J. Chem. Eng. Data. 60 (2015) 336–342. https://doi.org/10.1021/je500591q

47 U. Ranieri, M. M. Koza, W. F. Kuhs, S. Klotz, A. Falenty, P. Gillet and L. E. Bove, Fast methane diffusion at the interface of two clathrate structures, Nat. Commun. 8 (2017) 1–7. https://doi.org/10.1038/s41467-017-01167-2

48 A. Siangsai, P. Rangsunvigit, B. Kitiyanan, S. Kulprathipanja and P. Linga, Investigation on the roles of activated carbon particle sizes on methane hydrate formation and dissociation, Chem. Eng. Sci. 126 (2015) 383–389. https://doi.org/10.1016/j.ces.2014.12.047

49 Y. Jin, Y. Konno and J. Nagao, Growth of methane clathrate hydrates in porous media, Energy and Fuels. 26 (2012) 2242–2247. https://doi.org/10.1021/ef3001357

50 L. C. Jacobson, W. Hujo and V. Molinero, Amorphous precursors in the nucleation of clathrate hydrates, J. Am. Chem. Soc. 132 (2010) 11806–11811. https://doi.org/10.1021/ja1051445

51 L. C. Jacobson and V. Molinero, Can amorphous nuclei grow crystalline clathrates? the size and crystallinity of critical clathrate nuclei, J. Am. Chem. Soc. 133 (2011) 6458–6463. https://doi.org/10.1021/ja201403q

52 L. Wan, X. Zhou, P. Chen, X. Zang, D. Liang and J. Guan, Decomposition characterizations of methane hydrate confined inside nanoscale pores of silica gel below 273.15 K, Crystals. 9 (2019) 200. https://doi.org/10.3390/cryst9040200

53 A. K. Sum, R. C. Burruss and E. D. Sloan, Measurement of Clathrate Hydrates via Raman Spectroscopy, J. Phys. Chem. B, 101 (1997) 7371–7377. https://doi.org/10.1021/jp970768e

54 M. Kida, A. Hachikubo, H. Sakagami, H. Minami, A. Krylov, S. Yamashita, N. Takahashi, H. Shoji, O. Khlystov, J. Poort and H. Narita, Natural gas hydrates with locally different cage occupancies and hydration numbers in Lake Baikal, Geochem. Geophys. Geosyst. 10 (2009) . https://doi.org/10.1029/2009GC002473

55 A. M. M. Bustin, R. M. Bustin, I. L. Moudrakovskim, S. Takeya and J. A. Ripmeester, Formation of Methane Clathrate Hydrates in Coal Moisture: Implications for Coalbed Methane Resources and Reservoir Pressures, Energy and Fuels. 30 (2016) 88–97. https://doi.org/10.1021/acs.energyfuels.5b01922

56 K. Ishikiriyama and M. Todoki, Evaluation of water in silica pores using differential scanning calorimetry, Thermochim. Acta. 256 (1995) 213–226. https://doi.org/10.1016/0040-6031(94)02174-M

57 Y. P. Handa, Calorimetric determinations of the compositions, enthalpies of dissociation, and heat capacities in the range 85 to 270 K for clathrate hydrates of xenon and krypton, J. Chem. Thermodyn. 18 (1986) 891–902. https://doi.org/10.1016/0021-9614(86)90124-2